

Article

New Type-I and Type-II Clathrates in the Systems Cs–Na–Ga–Si, Rb–Na–Ga–Si, and Rb–Na–Zn–Si

Marion C. Schäfer and Svilen Bobev *

Department of Chemistry & Biochemistry, University of Delaware, Newark, DE 19716, USA;
E-Mail: schaefer@udel.edu

* Author to whom correspondence should be addressed; E-Mail: bobev@udel.edu;
Tel.: +1-302-831-8720; Fax: +1-302-831-6335.

Received: 14 January 2014; in revised form: 25 February 2014 / Accepted: 28 February 2014 /
Published: 18 March 2014

Abstract: Systematic studies in the systems Cs–Na–Ga–Si, Rb–Na–Ga–Si, and Rb–Na–Zn–Si yielded the novel type-I clathrates with refined compositions $\text{Cs}_6\text{Na}_2\text{Ga}_{8.25}\text{Si}_{37.75(3)}$, $\text{Rb}_{6.34}\text{Na}_{1.66(2)}\text{Ga}_{8.02}\text{Si}_{37.98(3)}$, and $\text{Rb}_{5.20}\text{Na}_{2.80(4)}\text{Zn}_{3.85}\text{Si}_{42.15(2)}$ (cubic, $Pm\bar{3}n$), as well as the type-II clathrates with formulae $\text{Cs}_8\text{Na}_{16}\text{Ga}_{22.7}\text{Si}_{113.3(1)}$, $\text{Rb}_{8.4}\text{Na}_{15.6(1)}\text{Ga}_{19.6}\text{Si}_{116.4(1)}$, and $\text{Rb}_8\text{Na}_{16}\text{Zn}_{8.4}\text{Si}_{127.6(1)}$ (cubic, $Fd\bar{3}m$). In each system, the type-I and -II compounds are always co-crystallizing, irrespective of the reaction conditions. The structures derived from single-crystal X-ray diffraction confirm complete ordering of Cs and Na atoms, and nearly complete ordering of the Rb and Na guest atoms. The framework-building Si atoms are randomly substituted by Ga or Zn atoms on all framework sites with notable difference in the substitution patterns between the type-I and type-II structure. This, and other details of the crystal chemistry are discussed in this paper.

Keywords: clathrates; type-I structure; type-II structure; silicon

1. Introduction

Clathrates of the group 14 elements have already been known for five decades, being named in analogy to the gas hydrates $G_8(\text{H}_2\text{O})_{36}$ and $G_{24}(\text{H}_2\text{O})_{136}$ ($G = \text{Xe}, \text{Cl}_2, \text{CH}_4, \text{etc.}$) [1]. The interest in such compounds with open-framework structures has grown from a point of laboratory curiosity to a heavily studied subset of materials with a large potential for thermoelectric energy conversion [2–5] according to the Phonon-glass Electron-crystal (PGEC) concept, proposed by Slack about 20 years

ago [2]. The basis of Slack's idea is the clathrate framework, made up of covalently-bound Si, Ge or Sn atoms, which imparts structural rigidity and ensures high electron mobilities, while the guest atoms residing in the somewhat oversized cages (often referred to as "fillers" and/or "rattlers"), contribute to lattice-vibrations that can lower the lattice component of the thermal conductivity.

As mentioned already, most known clathrate compounds are based on the group 14 elements Si, Ge and Sn (Tetrel or *Tt*, as denoted hereafter) and predominantly crystallize into two structure types (out of *ca.* 10 possible [1]). These *Tt*-framework atoms are tetrahedrally coordinated and can be substituted by group 13 and 12 elements, as well as late transition metals (*M*), and the resulting cages are partially or fully occupied by guest atoms (*A*), such as alkali metals, alkaline-earth metals, or the rare-earth metals Ce and Eu [6–9]. The most common structure for the clathrates is type-I with the nominal composition $A_8(M,Tt)_{46}$ followed by type-II with the general formula $A_{24}(M,Tt)_{136}$. The structure of type-I boasts 20- and 24-atom cages, while the structure of the type-II clathrates is based upon 20- and 28-atom polyhedra. Due to these differences in their frameworks, for the type-I compounds, a complete occupation of all cages can be achieved either with one or two kinds of guest atoms, e.g., (K or Rb)₈Ga₈Si₃₈ [10,11], K₆Eu₂Ga₁₀Ge₃₆ [12], K₆Eu₂(Zn or Cd)₅Ge₄₁ [12], Rb₈In₈Ge₃₈ [13], and (Rb,Eu)₈In_xGe_{46-x} [14], while two types of different guest atoms will be preferred for the complete and ordered filling of both cavities in the type-II compounds. Some examples, illustrating this line of thinking, are (Cs or Rb)₈Na₁₆(Si or Ge)₁₃₆ [6,15,16], Cs₈Na₁₆Ga₂₁Si₁₁₅ [17], Rb_{7.3}Na₁₆Ga₂₀Si₁₁₆ [17], Cs₈Na₁₆Ag_{6.7}Ge_{129.3} [18], Cs₈Na₁₆Cu₅Ge₁₃₁ [19], Cs₈Ba₁₆Ga_{39.7}Sn_{96.3} [20], and Rb_{9.9}Ba_{13.3}Ga_{36.4}Sn_{99.6} [20]. The near complete filling of both cages in the type-II structure by a single guest atom, as shown in the example of Na_{24-x}Si₁₃₆ ($0 \leq x \leq 24$) has recently been also proven possible, however, it is apparently concomitant with substantial disorder of the Na atoms in the large Si₂₈ cages [21–23].

While the crystal chemistry and the chemical bonding in most of the clathrate structures are satisfactorily understood today, the difficulty to synthesize selectively new compounds of each type remains largely unsolved [24]. This is caused by the nearly same thermodynamic stability of the known clathrate types and the remarkably similar chemical compositions. This becomes clearer if the ratios of framework atoms to guest atoms are considered, e.g., the ratio of the type-II compounds $A_{24}(M,Tt)_{136}$ are 24:136 or 1:5.67 compared to the ratio for type-I clathrates $A_8(M,Tt)_{46}$ of 8:46 or 1:5.75. The cavities of the former one have a larger difference in size; therefore, a directed synthesis should be possible with choosing different guest atoms combined with the "right" *M*-substituted framework. Based on this hypothesis, we carried out investigations in the systems Cs–Na–Ga–Si, Rb–Na–Ga–Si, and Rb–Na–Zn–Si, and the resulting type-I and type-II clathrates are presented in this report.

2. Results and Discussion

2.1. Synthesis

In 2006, we reported for the very first time the occurrence of the type-II clathrates Cs₈Na₁₆Ga₂₁Si₁₁₅ and Rb_{7.3}Na₁₆Ga₂₀Si₁₁₆ [17]. We set out to optimize the syntheses for possible measurements of the transport properties. The syntheses were carried out as stoichiometric reactions in Nb tubes and a very slow heating rate of 10 °C to 950 °C was found to be mandatory for the best results. However, for both

systems, always a mixture of type-II and type-I clathrates were obtained, namely the Cs containing compounds $\text{Cs}_8\text{Na}_{16}\text{Ga}_{22.7}\text{Si}_{113.3(1)}$ and $\text{Cs}_6\text{Na}_2\text{Ga}_{8.25}\text{Si}_{37.75(3)}$, and the Rb-containing clathrates $\text{Rb}_{8.4}\text{Na}_{15.6(1)}\text{Ga}_{19.6}\text{Si}_{116.4(1)}$ and $\text{Rb}_{6.34}\text{Na}_{1.66(2)}\text{Ga}_{8.02}\text{Si}_{37.98(3)}$, together with some left-over Si. The clathrate phases cannot be distinguished due to the same physical appearance of the respective crystals—cuboidal shape and dark color, their similar stability in acids and bases prevented the use of chemical agents as well. Using induction heating or flux methods (see experimental) did not improve the reaction outcomes. When we tried to replace Ga as framework substituting atoms with Zn, the type-II clathrate $\text{Rb}_8\text{Na}_{16}\text{Zn}_{8.4}\text{Si}_{127.6(1)}$ and the type-I clathrate $\text{Rb}_{5.20}\text{Na}_{2.80(4)}\text{Zn}_{3.85}\text{Si}_{42.15(2)}$ were obtained. Here, again, both kinds of clathrates are also occurring simultaneously, and a separation was once more not possible.

Table 1. Selected crystal data and structure refinement parameters for $\text{Cs}_8\text{Na}_{16}\text{Ga}_{22.7}\text{Si}_{113.3(1)}$ (**1**), $\text{Rb}_{8.4}\text{Na}_{15.6(1)}\text{Ga}_{19.6}\text{Si}_{116.4(1)}$ (**2**), and $\text{Rb}_8\text{Na}_{16}\text{Zn}_{8.4}\text{Si}_{127.6(1)}$ (**3**).

| Compound | 1 | 2 | 3 |
|--|--|----------------|----------------|
| Fw/g/mol | 6196.36 | 5707.57 | 5184.99 |
| Crystal system | Cubic | | |
| Space group | $Fd\bar{3}m$ (No. 227) | | |
| $a/\text{Å}$ | 14.9354(5) | 14.8822(10) | 14.8027(10) |
| $V/\text{Å}^3$ | 3331.6(2) | 3296.1(4) | 3243.6(4) |
| Z | 1 | | |
| T/K | 200(2) | | |
| Radiation | $\text{MoK}\alpha$, $\lambda = 0.71073 \text{ Å}$ | | |
| $\rho/\text{g}\cdot\text{cm}^{-3}$ | 3.09 | 2.88 | 2.65 |
| μ/cm^{-1} | 7.76 | 8.13 | 5.78 |
| R_{int} | 0.037 | 0.101 | 0.108 |
| data/restraints/parameters | 233/0/16 | 242/0/17 | 235/0/17 |
| $R_1 [I > 2\sigma(I)]^{[a]}$ | 0.0170 | 0.0238 | 0.0294 |
| $wR_2 [I > 2\sigma(I)]^{[a]}$ | 0.0485 | 0.0522 | 0.0588 |
| GOF | 1.162 | 1.115 | 1.086 |
| largest peak & hole/ $e^{-}\cdot\text{Å}^{-3}$ | 0.88 & -0.30 | 0.56 & -0.47 | 0.75 & -0.66 |

^[a] $R_1 = \sum||F_o| - |F_c||/\sum|F_o|$; $wR_2 = [\sum[w(F_o^2 - F_c^2)^2]/\sum[w(F_o^2)^2]]^{1/2}$, where $w = 1/[\sigma^2 F_o^2 + (A \cdot P)^2 + (B \cdot P)]$, and $P = (F_o^2 + 2F_c^2)/3$; A and B weight coefficients.

2.2. Crystal Chemistry of the Type-II Clathrates

The unit cells of the three cubic type-II clathrates (space group $Fd\bar{3}m$, see Table 1) decrease at 200 K from $a = 14.9354(5) \text{ Å}$ for $\text{Cs}_8\text{Na}_{16}\text{Ga}_{22.7}\text{Si}_{113.3(1)}$ (**1**), to $a = 14.8822(10) \text{ Å}$ for $\text{Rb}_{8.4}\text{Na}_{15.6(1)}\text{Ga}_{19.6}\text{Si}_{116.4(1)}$ (**2**), to $a = 14.8027(10) \text{ Å}$ for $\text{Rb}_8\text{Na}_{16}\text{Zn}_{8.4}\text{Si}_{127.6(1)}$ (**3**). This reduction is in agreement with the observed decreased amount of Ga in **1** vs. **3**; the relatively larger difference in the unit cell volumes of **2** vs. **3** can be attribute to the larger size of the atoms Ga compared to Zn ($r_{\text{Ga}} \approx 1.25 \text{ Å}$, $r_{\text{Zn}} \approx 1.21 \text{ Å}$, $r_{\text{Si}} \approx 1.17 \text{ Å}$, according to Pauling [25]). The guest atoms must also have an effect, but it appears to be more subtle (the difference in the metallic radii for the alkali metal Cs and Rb is quite large, $r_{\text{Cs}} \approx 2.35 \text{ Å}$, $r_{\text{Rb}} \approx 2.16 \text{ Å}$ according to Pauling [25]). As both Zn and Ga are larger than Si, any substitutions to the framework result in enlargement of the unit cell, clearly seen by comparing our

data with the data for the known ternary type-II clathrates $\text{Cs}_8\text{Na}_{16}\text{Si}_{136}$ [15] and $\text{Rb}_8\text{Na}_{16}\text{Si}_{136}$ [6] have with $a = 14.7560(4)$ Å and $a = 14.7400(4)$ Å, respectively.

The compositions of the previously reported type-II compounds $\text{Cs}_8\text{Na}_{16}\text{Ga}_{21}\text{Si}_{115}$ and $\text{Rb}_{7.3}\text{Na}_{16}\text{Ga}_{20}\text{Si}_{116}$ [17] and the herein reported **1** and **2** are worth considering too. Note that from the structure refinements, the Ga-substitution rates appear rather similar, with the new Cs-containing phase **1** having slightly higher amount of Ga than in the earlier reported $\text{Cs}_8\text{Na}_{16}\text{Ga}_{21}\text{Si}_{115}$. This conjecture can be seen by comparing the corresponding unit cells as well— $\text{Cs}_8\text{Na}_{16}\text{Ga}_{21}\text{Si}_{115}$ has a cell parameter of $a = 14.918(2)$ Å, which expand slightly to $a = 14.9354(5)$ Å for $\text{Cs}_8\text{Na}_{16}\text{Ga}_{22.7}\text{Si}_{113.3(1)}$, in a manner consistent with the increased Ga-content (the unit cell difference might actually be smaller due to the fact that the previous measurement was taken at 120 K, while the current is at 200 K). The comparison of the Rb-containing compounds shows nearly identical cell parameter with $a = 14.883(2)$ Å for $\text{Rb}_{7.3}\text{Na}_{16}\text{Ga}_{20}\text{Si}_{116}$ and $a = 14.8822(10)$ Å for $\text{Rb}_{8.4}\text{Na}_{15.6(1)}\text{Ga}_{19.6}\text{Si}_{116.4(1)}$. Interpretation of this result is hindered again by the different temperatures at which the unit cell parameters have been determined. The slight discrepancy in the refined formulae with regard to the alkali metals is another issue to be considered (*vide infra*).

The open-framework of the type-II clathrates comprises of 136 tetrahedrally coordinated M and Si atoms ($M = \text{Ga}, \text{Zn}$) per unit cell located on the Wyckoff sites $96g$, $32e$, and $8a$. The structure is best viewed as constituting a space-filling network of 16 $(M,\text{Si})_{20}$ pentagonal dodecahedra and 8 $(M,\text{Si})_{28}$ hexakaidecahedra (see Figure 1). The larger 28-atom polyhedra are linked in a diamond-like fashion via their four hexagonal faces, while the smaller 20-atom polyhedra generate face-shared layers running along $[111]$ in ABC-sequence, typical for the face-centered cubic symmetry. In the herein presented Si-based clathrates, the framework is substituted with Ga and Zn, respectively, and the framework site $96g$ is favored by these larger atoms, while site $8a$ is the least preferred site. This is visible in the atom contribution (see Tables 2 and 3) with Si:(Ga,Zn) ratios of 78:22 for **1**, 82:18 for **2** and 92:8 for **3** on $96g$, 96:4 for **1**, 94:6 for **2** and 98:2 for **3** on $32e$, and 97:3 for **1** and 96:1 for **2** on $8a$. Only Si is occupying site $8a$ in the Zn-containing compound **3**. The same trend is occurring as well in both known Ga-substituted type-II clathrates $\text{Cs}_8\text{Na}_{16}\text{Ga}_{21}\text{Si}_{115}$ (ratio Si:Ga is 80:20 on $96g$, 95:5 on $32e$, and 98:2 on $8a$) and $\text{Rb}_{7.3}\text{Na}_{16}\text{Ga}_{20}\text{Si}_{116}$ (ratio Si:Ga is 80:20 on $96g$, 96:4 on $32e$, and 99:1 on $8a$) with comparable ratios. In all cases, the larger substituted anions increase the cage sizes and therefore an expansion of the unit cells (*vide supra*) occur in accordance with the increasing amount of incorporated Zn and Ga, respectively. This can be also observed in the atomic distances (see Table 4), which fall in the intervals of $d_{\text{Si/Ga-Si/Ga}} = 2.385(1)$ to $2.430(1)$ Å for **1**, $d_{\text{Si/Ga-Si/Ga}} = 2.380(1)$ to $2.423(1)$ Å for **2**, and $d_{\text{Si/Zn-Si/Zn}} = 2.373(1)$ to $2.412(1)$ Å for **3**, respectively. The distances in $\text{Cs}_8\text{Na}_{16}\text{Ga}_{21}\text{Si}_{115}$ ($d_{\text{Si/Ga-Si/Ga}} = 2.386(1)$ – $2.428(2)$ Å) and $\text{Rb}_{7.3}\text{Na}_{16}\text{Ga}_{20}\text{Si}_{116}$ ($d_{\text{Si/Ga-Si/Ga}} = 2.378(1)$ – $2.426(2)$ Å) [17] also agree well. As expected, all distance have longer values than these for the ternary clathrates $\text{Cs}_8\text{Na}_{16}\text{Si}_{136}$ ($d_{\text{Si-Si}} = 2.3584(4)$ – $2.3924(5)$ Å at room temperature) [15] and $\text{Rb}_8\text{Na}_{16}\text{Si}_{136}$ ($d_{\text{Si-Si}} = 2.362(1)$ – $2.395(1)$ Å at room temperature) [6].

Figure 1. View of the polyanionic framework of clathrates with type-II structure (yellow: pentagonal dodecahedra; red: hexakaidecahedra).

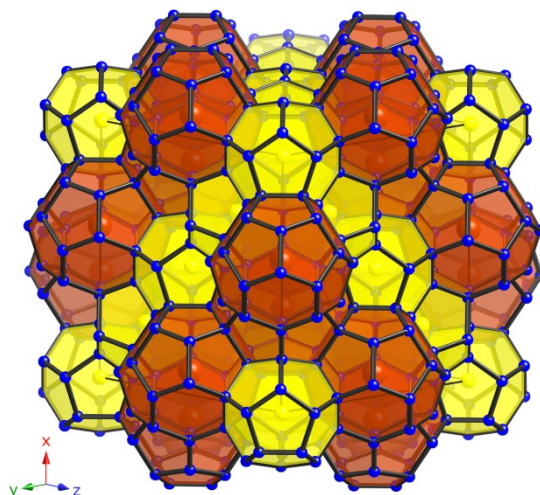


Table 2. Atomic coordinates and equivalent isotropic displacement parameters ($U_{eq}/\text{\AA}^2$) for $\text{Cs}_8\text{Na}_{16}\text{Ga}_{22.7}\text{Si}_{113.3(1)}$ (**1**); $\text{Rb}_{8.4}\text{Na}_{15.6(1)}\text{Ga}_{19.6}\text{Si}_{116.4(1)}$ (**2**); and $\text{Rb}_8\text{Na}_{16}\text{Zn}_{8.4}\text{Si}_{127.6(1)}$ (**3**). Coordinates are reported in the origin choice No. 2 for the cubic space group $Fd\bar{3}m$.

| Atom | site | x/a | y/b | z/c | occupancy/% | U_{eq} ^[a] |
|--|------|---------------|---------------|---------------|----------------------|-------------------------|
| $\text{Cs}_8\text{Na}_{16}\text{Ga}_{22.7}\text{Si}_{113.3(1)}$ | | | | | | |
| Na | 16c | 0 | 0 | 0 | 100 | 0.0212(6) |
| Cs | 8b | $\frac{3}{8}$ | $\frac{3}{8}$ | $\frac{3}{8}$ | 100 | 0.0205(2) |
| Si1/Ga1 | 96g | 0.06746(2) | x | 0.37069(3) | 78/22 ^[b] | 0.0087(2) |
| Si2/Ga2 | 32e | 0.21719(4) | x | x | 95.6/4.4(4) | 0.0079(4) |
| Si3/Ga3 | 8a | $\frac{1}{8}$ | $\frac{1}{8}$ | $\frac{1}{8}$ | 96.8/3.3(7) | 0.0084(7) |
| $\text{Rb}_{8.4}\text{Na}_{15.6(1)}\text{Ga}_{19.6}\text{Si}_{116.4(1)}$ | | | | | | |
| Na1/Rb1 | 16c | 0 | 0 | 0 | 97.9/2.1(7) | 0.020(1) |
| Rb2 | 8b | $\frac{3}{8}$ | $\frac{3}{8}$ | $\frac{3}{8}$ | 100 | 0.0283(4) |
| Si1/Ga1 | 96g | 0.06734(3) | x | 0.37088(5) | 82/18 ^[b] | 0.0084(2) |
| Si2/Ga2 | 32e | 0.21728(6) | x | x | 93.9/6.1(5) | 0.0083(5) |
| Si3/Ga3 | 8a | $\frac{1}{8}$ | $\frac{1}{8}$ | $\frac{1}{8}$ | 96/4(1) | 0.0078(9) |
| $\text{Rb}_8\text{Na}_{16}\text{Zn}_{8.4}\text{Si}_{127.6(1)}$ | | | | | | |
| Na | 16c | 0 | 0 | 0 | 100 | 0.0212(10) |
| Rb | 8b | $\frac{3}{8}$ | $\frac{3}{8}$ | $\frac{3}{8}$ | 100 | 0.0296(5) |
| Si1/Zn1 | 96g | 0.06740(4) | x | 0.37091(6) | 92/8 ^[b] | 0.0086(3) |
| Si2/Zn2 | 32e | 0.21755(7) | x | x | 97.6/2.4(6) | 0.0087(4) |
| Si3 | 8a | $\frac{1}{8}$ | $\frac{1}{8}$ | $\frac{1}{8}$ | 100 | 0.0074(7) |

^[a] U_{eq} is defined as one third of the trace of the orthogonalized U_{ij} tensor; ^[b] As this is the largest contributor to error, the occupancy at the 96g site was refined freely first, and then fixed in order to minimize the estimated standard deviation in the chemical formulae.

Table 3. Anisotropic displacement parameters ($U_{ij}/\text{\AA}^2$) for $\text{Cs}_8\text{Na}_{16}\text{Ga}_{22.7}\text{Si}_{113.3(1)}$ (**1**); $\text{Rb}_{8.4}\text{Na}_{15.6(1)}\text{Ga}_{19.6}\text{Si}_{116.4(1)}$ (**2**); and $\text{Rb}_8\text{Na}_{16}\text{Zn}_{8.4}\text{Si}_{127.6(1)}$ (**3**).

| Atom | U_{11} | U_{22} | U_{33} | U_{23} | U_{13} | U_{12} |
|--|------------|------------|------------|-------------|------------|------------|
| $\text{Cs}_8\text{Na}_{16}\text{Ga}_{22.7}\text{Si}_{113.3(1)}$ | | | | | | |
| Na | 0.0212(6) | = U_{11} | = U_{11} | -0.0031(6) | = U_{23} | = U_{23} |
| Cs | 0.0205(2) | = U_{11} | = U_{11} | 0 | 0 | 0 |
| Si1/Ga1 | 0.0086(2) | = U_{11} | 0.0091(3) | -0.0001(1) | = U_{23} | 0.0003(2) |
| Si2/Ga2 | 0.0079(4) | = U_{11} | = U_{11} | 0.0001(2) | = U_{23} | = U_{23} |
| Si3/Ga3 | 0.0084(7) | = U_{11} | = U_{11} | 0 | 0 | 0 |
| $\text{Rb}_{8.4}\text{Na}_{15.6(1)}\text{Ga}_{19.6}\text{Si}_{116.4(1)}$ | | | | | | |
| Na1/Rb1 | 0.0233(7) | = U_{11} | = U_{11} | -0.0013(8) | = U_{23} | = U_{23} |
| Rb2 | 0.0299(4) | = U_{11} | = U_{11} | 0 | 0 | 0 |
| Si1/Ga1 | 0.0082(3) | = U_{11} | 0.0089(4) | -0.0003(2) | = U_{23} | 0.0002(3) |
| Si2/Ga2 | 0.0080(3) | = U_{11} | = U_{11} | 0.0007(3) | = U_{23} | = U_{23} |
| Si3/Ga3 | 0.0075(4) | = U_{11} | = U_{11} | 0 | 0 | 0 |
| $\text{Rb}_8\text{Na}_{16}\text{Zn}_{8.4}\text{Si}_{127.6(1)}$ | | | | | | |
| Na | 0.0212(10) | = U_{11} | = U_{11} | -0.0025(10) | = U_{23} | = U_{23} |
| Rb | 0.0296(5) | = U_{11} | = U_{11} | 0 | 0 | 0 |
| Si1/Zn1 | 0.0083(4) | = U_{11} | 0.0093(5) | 0.0001(2) | = U_{23} | 0.0000(3) |
| Si2/Zn2 | 0.0087(4) | = U_{11} | = U_{11} | 0.0005(4) | = U_{23} | = U_{23} |
| Si3 | 0.0074(7) | = U_{11} | = U_{11} | 0 | 0 | 0 |

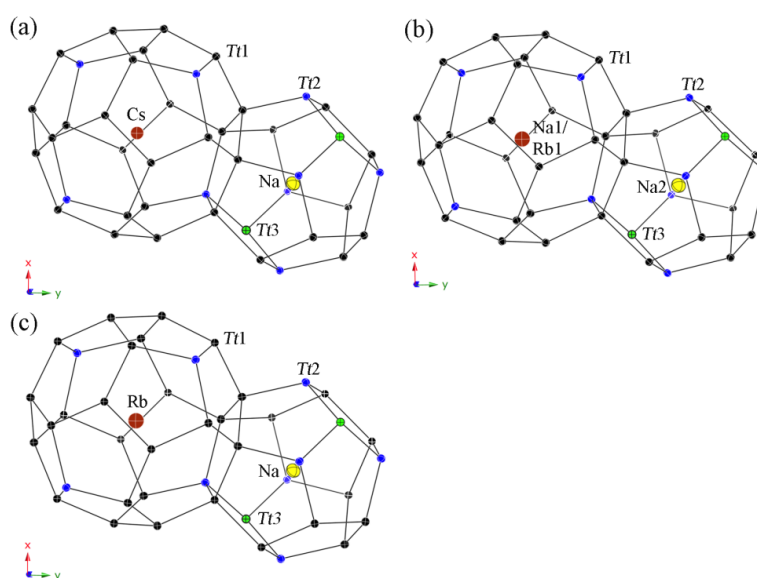
Table 4. Selected interatomic distances for $\text{Cs}_8\text{Na}_{16}\text{Ga}_{22.7}\text{Si}_{113.3(1)}$ (**1**); $\text{Rb}_{8.4}\text{Na}_{15.6(1)}\text{Ga}_{19.6}\text{Si}_{116.4(1)}$ (**2**); and $\text{Rb}_8\text{Na}_{16}\text{Zn}_{8.4}\text{Si}_{127.6(1)}$ (**3**). *Tt* denotes the mixed occupied Si/Ga and Si/Zn, respectively.

| Compound 1 | $d/\text{\AA}$ | Compound 2 | $d/\text{\AA}$ | Compound 3 | $d/\text{\AA}$ |
|-------------------------------|----------------|------------------------------------|----------------|-------------------------------|----------------|
| <i>Tt1-Tt1</i> (2 \times) | 2.4016(5) | <i>Tt1-Tt1</i> (2 \times) | 2.3894(8) | <i>Tt1-Tt1</i> (2 \times) | 2.377(1) |
| <i>Tt1-Tt2</i> | 2.4067(5) | <i>Tt1-Tt2</i> | 2.3989(8) | <i>Tt1-Tt2</i> | 2.385(1) |
| <i>Tt1-Tt1</i> | 2.430(1) | <i>Tt1-Tt1</i> | 2.437(1) | <i>Tt1-Tt1</i> | 2.412(2) |
| <i>Tt2-Tt3</i> | 2.3847(9) | <i>Tt2-Tt3</i> | 2.380(1) | <i>Tt2-Si3</i> | 2.373(2) |
| <i>Tt2-Tt1</i> (3 \times) | 2.4066(5) | <i>Tt2-Tt1</i> (3 \times) | 2.3988(8) | <i>Tt2-Tt1</i> (3 \times) | 2.385(1) |
| <i>Tt3-Tt2</i> (4 \times) | 2.3847(9) | <i>Tt3-Tt2</i> (4 \times) | 2.379(1) | <i>Si3-Tt2</i> (4 \times) | 2.373(2) |
| Na- <i>Tt3</i> (2 \times) | 3.2336(1) | Na1/Rb1- <i>Tt3</i> (2 \times) | 3.2221(2) | Na-Si3 (2 \times) | 3.2049(2) |
| Na- <i>Tt2</i> (6 \times) | 3.3140(4) | Na1/Rb1- <i>Tt2</i> (6 \times) | 3.3066(6) | Na- <i>Tt2</i> (6 \times) | 3.2912(7) |
| Na- <i>Tt1</i> (12 \times) | 3.4260(3) | Na1/Rb1- <i>Tt1</i> (12 \times) | 3.4102(5) | Na- <i>Tt1</i> (12 \times) | 3.3939(6) |
| Cs- <i>Tt1</i> (12 \times) | 3.9879(4) | Rb2- <i>Tt1</i> (12 \times) | 3.9719(7) | Rb- <i>Tt1</i> (12 \times) | 3.950(1) |
| Cs- <i>Tt1</i> (12 \times) | 4.0657(5) | Rb2- <i>Tt1</i> (12 \times) | 4.049(1) | Rb- <i>Tt1</i> (12 \times) | 4.028(1) |
| Cs- <i>Tt2</i> (4 \times) | 4.0825(9) | Rb2- <i>Tt2</i> (4 \times) | 4.064(1) | Rb- <i>Tt2</i> (4 \times) | 4.037(2) |

Due to the very different sizes of the two kinds of polyhedra, two very different guest atoms are required in order to achieve the complete and ordered occupation of the respective cages (see Figure 2). This warranted our choice of the pairs of alkali metals, namely Na/Cs and Na/Rb, respectively ($r_{\text{Na}} \approx 1.57 \text{ \AA}$, $r_{\text{Rb}} \approx 2.16 \text{ \AA}$, $r_{\text{Cs}} \approx 2.35 \text{ \AA}$ [25]). The optimal sizes for an ordering are realized with Na for the smaller pentagon dodecahedra and Cs for the larger hexakaidecahedra in **1** and in $\text{Cs}_8\text{Na}_{16}\text{Ga}_{21}\text{Si}_{115}$ [17] and as well with Na again in the $(\text{Si,Zn})_{20}$ cages and Rb in the $(\text{Si,Zn})_{28}$ cages

in compound **3**. In contrast, the Ga-substituted framework of the Rb-containing clathrate **2** is intermediate in size (between **1** and **3**), therefore, one can surmise that the larger cavities will still favor occupation by Rb atoms only, while the smaller ones are now large enough to host Na atoms, admixed with a small amount of Rb (refined as statistical ratio of Na:Rb = 97:3). For comparison, in $\text{Rb}_{7.3}\text{Na}_{16}\text{Ga}_{20}\text{Si}_{116}$ [17], the pentagonal dodecahedra are fully occupied by Na, while the hexakaidecahedra are only 90% occupied by the Rb guest atoms, despite the similar amount of Ga substituting for Si in the framework and the correspondingly similar sizes of the $(\text{Ga},\text{Si})_{20}$ pentagonal dodecahedra and the $(\text{Ga},\text{Si})_{28}$ hexakaidecahedra (between $\text{Rb}_{7.3}\text{Na}_{16}\text{Ga}_{20}\text{Si}_{116}$ [17] and structure **2**). We were intrigued by this difference in the filling patterns for $\text{Rb}_{8.4}\text{Na}_{15.6(1)}\text{Ga}_{19.6}\text{Si}_{116.4(1)}$ and the previously reported $\text{Rb}_{7.3}\text{Na}_{16}\text{Ga}_{20}\text{Si}_{116}$ [17]. We speculated that differences in the reaction conditions might explain why this happens, and attempted to synthesize a new clathrate type-II from Rb, Na, Ga, and Si, using a modified synthetic procedure. Several random crystals selected from this reaction were subjected to crystallographic analysis and showed again the exact same phenomenology—one crystal was indexed with a unit cell $a = 14.8722(5)$ Å, and another one with $a = 14.8765(5)$ Å, both at 200 K. Despite these values being within a few standard deviations from each other, structure refinements showed the former to be an analog of **2**, *i.e.*, the structure with the small Na-Rb disorder within the pentagonal dodecahedra, while the latter turned out to be analogous to the previously reported Rb–Na–Ga–Si phase with underoccupied hexakaidecahedral cages. The slight decrease in the unit cell parameters for these two structures compared to $\text{Rb}_{8.4}\text{Na}_{15.6(1)}\text{Ga}_{19.6}\text{Si}_{116.4(1)}$ and $\text{Rb}_{7.3}\text{Na}_{16}\text{Ga}_{20}\text{Si}_{116}$ is apparently due to the slight difference in the Ga content (an artifact of the change in the synthesis scheme). Based on the above, it is evident that the Rb–Na–Ga–Si system requires more detailed studies to fully understand this behavior, which is not mirrored by the analogous Cs–Na–Ga–Si system.

Figure 2. Representation of the polyhedral cages in type-II structures with anisotropic displacement parameters, drawn at the 95% probability level. $\text{Cs}_8\text{Na}_{16}\text{Ga}_{22.7}\text{Si}_{113.3(1)}$ (a); $\text{Rb}_{8.4}\text{Na}_{15.6(1)}\text{Ga}_{19.6}\text{Si}_{116.4(1)}$ (b); and $\text{Rb}_8\text{Na}_{16}\text{Zn}_{8.4}\text{Si}_{127.6(1)}$ (c).



The interatomic distances between the filler atoms and the framework are within the intervals of $d_{\text{Na-Si/Ga}} = 3.234(1)$ to $3.420(1)$ Å and $d_{\text{Cs-Si/Ga}} = 3.988(1)$ to $4.083(1)$ Å for **1**, $d_{\text{Na1/Rb1-Si/Ga}} = 3.222(1)$ to

3.410(1) Å and $d_{\text{Rb2-Si/Ga}} = 3.972(1)$ to 4.064(1) Å for **2**, and $d_{\text{Na-Si/Ga}} = 3.205(1)$ to 3.392(1) Å and $d_{\text{Rb-Si/Ga}} = 3.950(1)$ to 4.037(1) Å for **3**, respectively (see Table 4). The distances for $\text{Cs}_8\text{Na}_{16}\text{Ga}_{21}\text{Si}_{115}$ ($d_{\text{Na-Si/Ga}} = 3.230(1)$ –3.416(1) Å and $d_{\text{Cs-Si/Ga}} = 3.984(1)$ –4.077(2) Å) and $\text{Rb}_{7.3}\text{Na}_{16}\text{Ga}_{20}\text{Si}_{116}$ ($d_{\text{Na-Si/Ga}} = 3.222(1)$ –3.411(1) Å and $d_{\text{Rb-Si/Ga}} = 3.971(1)$ –4.066(2) Å) [17] are very close in values as well. According to the Zintl-Klemm rules [26,27], the formulae for charge balanced compounds are $[(\text{Cs or Rb})^+]_8[\text{Na}^+]_{16}[4b\text{-Ga}^{1-}]_{24}[4b\text{-Si}^0]_{112}$ for **1** and **2** and $[\text{Rb}^+]_8[\text{Na}^+]_{16}[4b\text{-Zn}^{2-}]_{12}[4b\text{-Si}^0]_{124}$ for **3**. Hence, the composition of the Cs-containing compound **1** is the closest to the ideal formula, and a semiconducting-like (heavily doped, or even poorly metallic) behavior can be expected, while these for both Rb-containing clathrates **2** and **3** are obviously not charge-balanced and a metallic behavior can be predicted for both phases. In support of this reasoning, we can cite the known germanium clathrates $\text{Cs}_8\text{Na}_{16}\text{Ag}_{6.7}\text{Ge}_{129.3}$ [18] and $\text{Cs}_8\text{Na}_{16}\text{Cu}_5\text{Ge}_{131}$ [19], whose formulae also deviate from the ideal, charge-balanced compositions.

2.3. Crystal Chemistry of the Type-I Clathrates

Like for the above reported type-II clathrates, the cell parameters for the individual type-I clathrates are also decreasing at 200 K with $a = 10.4710(2)$ Å for $\text{Cs}_6\text{Na}_2\text{Ga}_{8.25}\text{Si}_{37.75(3)}$ (**4**), to $a = 10.4466(4)$ for $\text{Rb}_{6.34}\text{Na}_{1.66(2)}\text{Ga}_{8.02}\text{Si}_{37.98(3)}$ (**5**), to $a = 10.3543(4)$ Å for $\text{Rb}_{5.20}\text{Na}_{2.80(4)}\text{Zn}_{3.85}\text{Si}_{42.15(2)}$ (**6**) corresponding to the amount of Ga or Zn in the Si-based framework and the used alkali metals as guest atoms (see Tables 5–7). The insertion of Na in $\text{Rb}_{6.34}\text{Na}_{1.66(2)}\text{Ga}_{8.02}\text{Si}_{37.98(3)}$ has very little influence on the unit cell, as evident by comparing it to that of the ternary compound $\text{Rb}_8\text{Ga}_8\text{Si}_{38}$ ($a = 10.469(2)$ Å at room temperature) [11], while the cell parameter for the Zn-containing clathrate is even significantly smaller than that of $\text{K}_8\text{Ga}_{7.9}\text{Si}_{38.1}$ ($a = 10.427(1)$ Å at room temperature) [10].

Table 5. Selected crystal data and structure refinement parameters for $\text{Cs}_6\text{Na}_2\text{Ga}_{8.25}\text{Si}_{37.75(3)}$ (**4**); $\text{Rb}_{6.34}\text{Na}_{1.66(2)}\text{Ga}_{8.02}\text{Si}_{37.98(3)}$ (**5**); and $\text{Rb}_{5.20}\text{Na}_{2.80(4)}\text{Zn}_{3.85}\text{Si}_{42.15(2)}$ (**6**).

| Compound | 4 | 5 | 6 |
|--|--------------------------------------|--------------|--------------|
| Fw/g/mol | 2479.03 | 2205.85 | 1944.48 |
| Crystal system | Cubic | | |
| Space group | $Pm\bar{3}n$ (No. 223) | | |
| $a/\text{Å}$ | 10.4710(2) | 10.4466(4) | 10.3543(4) |
| $V/\text{Å}^3$ | 1148.06(4) | 1140.05(8) | 1110.10(7) |
| Z | 1 | | |
| T/K | 200(2) | | |
| Radiation | MoK α , $\lambda = 0.71073$ Å | | |
| $\rho/\text{g}\cdot\text{cm}^{-3}$ | 3.59 | 3.21 | 2.91 |
| μ/cm^{-1} | 10.48 | 12.42 | 8.91 |
| R_{int} | 0.053 | 0.089 | 0.075 |
| data/restraints/parameters | 241/0/18 | 241/0/20 | 241/0/19 |
| $R_1 [I > 2\sigma(I)]^{[a]}$ | 0.0159 | 0.0167 | 0.0135 |
| $wR_2 [I > 2\sigma(I)]^{[a]}$ | 0.0394 | 0.0362 | 0.0295 |
| GOF | 1.202 | 1.072 | 1.128 |
| largest peak & hole/ $e^{-}\cdot\text{Å}^{-3}$ | 0.59 & -0.42 | 0.37 & -0.30 | 0.40 & -0.23 |

^[a] $R_1 = \sum ||F_o| - |F_c|| / \sum |F_o|$; $wR_2 = [\sum [w(F_o^2 - F_c^2)^2] / \sum [w(F_o^2)^2]]^{1/2}$, where $w = 1/[\sigma^2 F_o^2 + (A \cdot P)^2 + (B \cdot P)]$, and $P = (F_o^2 + 2F_c^2)/3$; A and B weight coefficients.

Table 6. Atomic coordinates and equivalent isotropic displacement parameters ($U_{eq}/\text{\AA}^2$) for $\text{Cs}_6\text{Na}_2\text{Ga}_{8.25}\text{Si}_{37.75(3)}$ (**4**), $\text{Rb}_{6.34}\text{Na}_{1.66(2)}\text{Ga}_{8.02}\text{Si}_{37.98(3)}$ (**5**), and $\text{Rb}_{5.20}\text{Na}_{2.80(4)}\text{Zn}_{3.85}\text{Si}_{42.15(2)}$ (**6**).

| Atom | Site | x/a | y/b | z/c | occupancy/% | $U_{eq}^{(a)}$ |
|---|------|------------|------------|------------|-------------|----------------|
| $\text{Cs}_6\text{Na}_2\text{Ga}_{8.25}\text{Si}_{37.75(3)}$ | | | | | | |
| Cs | 6d | $1/4$ | $1/2$ | 0 | 100 | 0.0131(2) |
| Na | 2a | 0 | 0 | 0 | 100 | 0.0176(13) |
| Si1/Ga1 | 24k | 0 | 0.30307(8) | 0.11830(8) | 86(1)/14(1) | 0.0069(2) |
| Si2/Ga2 | 16i | 0.18385(7) | x | x | 96(1)/4(1) | 0.0076(3) |
| Si3/Ga3 | 6c | $1/4$ | 0 | $1/2$ | 30(1)/70(1) | 0.0079(4) |
| $\text{Rb}_{6.34}\text{Na}_{1.66(2)}\text{Ga}_{8.02}\text{Si}_{37.98(3)}$ | | | | | | |
| Rb1 | 6d | $1/4$ | $1/2$ | 0 | 100 | 0.0159(2) |
| Na2/Rb2 | 2a | 0 | 0 | 0 | 83(1)/17(1) | 0.0120(6) |
| Si1/Ga1 | 24k | 0 | 0.30439(7) | 0.11798(7) | 85(1)/15(1) | 0.0079(2) |
| Si2/Ga2 | 16i | 0.18411(5) | x | x | 97(1)/3(1) | 0.0078(3) |
| Si3/Ga3 | 6c | $1/4$ | 0 | $1/2$ | 34(1)/66(1) | 0.0076(2) |
| $\text{Rb}_{5.20}\text{Na}_{2.80(4)}\text{Zn}_{3.85}\text{Si}_{42.15(2)}$ | | | | | | |
| Rb1/Na1 | 6d | $1/4$ | $1/2$ | 0 | 86(1)/14(1) | 0.0161(2) |
| Na2 | 2a | 0 | 0 | 0 | 100 | 0.0124(7) |
| Si1/Zn1 | 24k | 0 | 0.30472(6) | 0.11742(6) | 97(1)/3(1) | 0.0071(2) |
| Si2/Zn2 | 16i | 0.18363(4) | x | x | 98(1)/2(1) | 0.0067(3) |
| Si3/Zn3 | 6c | $1/4$ | 0 | $1/2$ | 54(1)/46(1) | 0.0074(2) |

^[a] U_{eq} is defined as one third of the trace of the orthogonalized U_{ij} tensor.

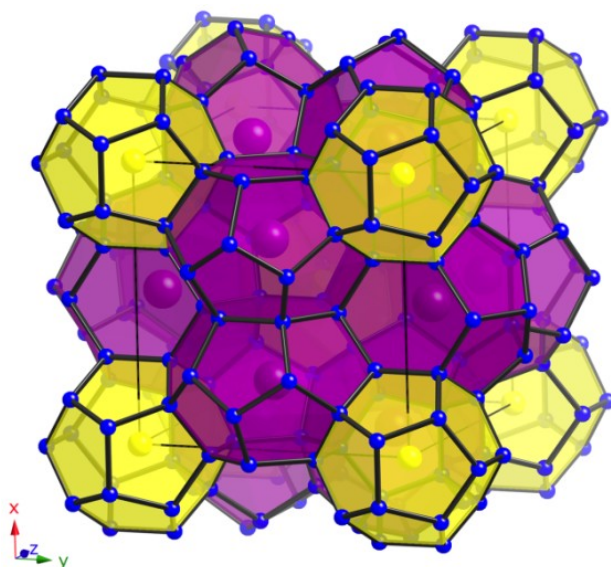
Table 7. Anisotropic displacement parameters ($U_{ij}/\text{\AA}^2$) for $\text{Cs}_6\text{Na}_2\text{Ga}_{8.25}\text{Si}_{37.75(3)}$ (**4**); $\text{Rb}_{6.34}\text{Na}_{1.66(2)}\text{Ga}_{8.02}\text{Si}_{37.98(3)}$ (**5**); and $\text{Rb}_{5.20}\text{Na}_{2.80(4)}\text{Zn}_{3.85}\text{Si}_{42.15(2)}$ (**6**).

| Atom | U_{11} | U_{22} | U_{33} | U_{23} | U_{13} | U_{12} |
|---|------------|-----------|-----------|------------|-----------|-----------|
| $\text{Cs}_6\text{Na}_2\text{Ga}_{8.25}\text{Si}_{37.75(3)}$ | | | | | | |
| Cs | 0.0098(3) | 0.0147(2) | $=U_{22}$ | 0 | 0 | 0 |
| Na | 0.0176(13) | $=U_{11}$ | $=U_{11}$ | 0 | 0 | 0 |
| Si1/Ga1 | 0.0060(4) | 0.0071(4) | 0.0077(4) | 0.0004(3) | 0 | 0 |
| Si2/Ga2 | 0.0076(3) | $=U_{11}$ | $=U_{11}$ | -0.0002(3) | $=U_{23}$ | $=U_{23}$ |
| Si3/Ga3 | 0.0080(5) | 0.0079(4) | $=U_{22}$ | 0 | 0 | 0 |
| $\text{Rb}_{6.34}\text{Na}_{1.66(2)}\text{Ga}_{8.02}\text{Si}_{37.98(3)}$ | | | | | | |
| Rb | 0.0116(4) | 0.0181(3) | $=U_{22}$ | 0 | 0 | 0 |
| Na/Rb1 | 0.0120(6) | $=U_{11}$ | $=U_{11}$ | 0 | 0 | 0 |
| Si1/Ga1 | 0.0077(4) | 0.0082(4) | 0.0077(4) | 0.0006(3) | 0 | 0 |
| Si2/Ga2 | 0.0078(3) | $=U_{11}$ | $=U_{11}$ | 0.0000(2) | $=U_{23}$ | $=U_{23}$ |
| Si3/Ga3 | 0.0080(5) | 0.0074(3) | $=U_{22}$ | 0 | 0 | 0 |
| $\text{Rb}_{5.20}\text{Na}_{2.80(4)}\text{Zn}_{3.85}\text{Si}_{42.15(2)}$ | | | | | | |
| Rb1/Na1 | 0.0124(3) | 0.0179(3) | $=U_{22}$ | 0 | 0 | 0 |
| Na2 | 0.0124(7) | $=U_{11}$ | $=U_{11}$ | 0 | 0 | 0 |
| Si1/Zn1 | 0.0065(4) | 0.0077(4) | 0.0069(3) | 0.0004(3) | 0 | 0 |
| Si2/Zn2 | 0.0067(3) | $=U_{11}$ | $=U_{11}$ | -0.0001(2) | $=U_{23}$ | $=U_{23}$ |
| Si3/Zn3 | 0.0081(4) | 0.0070(3) | $=U_{22}$ | 0 | 0 | 0 |

In the cubic type-I structure ($Pm\bar{3}n$) of these clathrates, statistically disordered Si and M atoms ($M = \text{Ga}, \text{Zn}$) form the open-framework with 46 tetrahedrally coordinated atoms per unit cell located on the Wyckoff sites 24k, 16i, and 6c. Overall, one unit cell encompasses two $(\text{Si}, M)_{20}$ pentagonal

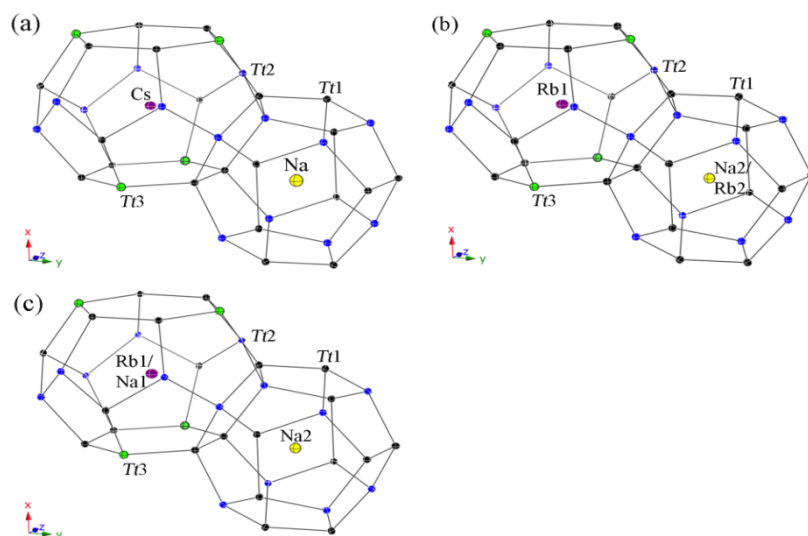
dodecahedra and six $(\text{Si},M)_{24}$ tetrakaidecahedra (see Figure 3) creating a space-filling network. The 24-atom polyhedra share their two hexagonal faces to create three perpendicular, but not interpenetrating columns running along $[100]$, $[010]$, and $[001]$ of the cube. These columns encapsulate the isolated 20-atom polyhedra in the created voids. The M atoms substitute all three framework sites in every clathrate (Table 6) with an apparent preference to occupy site $6c$. The ratios are in agreement with the literature, whereby the preference for the $6c$ site is confirmed. Our data show the following ratios—Si:Ga = 86:14 on $24k$, 96:4 on $16i$ and 30:70 on $6c$ for **4** and Si:Ga = 85:15 on $24k$, 97:3 on $16i$ and 34:66 on $6c$ for **5** similar and comparable to these of the ternary clathrates $\text{K}_8\text{Ga}_{7.9}\text{Si}_{38.1}$ (Si amounts in percents of the site occupation factors: 83%, 98%, and 43%, respectively) [10] and $\text{Rb}_8\text{Ga}_8\text{Si}_{38}$ (Si amounts in percents of the site occupation factors: 78%, 99%, and 59%, respectively) [11], while the ratio of Si:Zn = 97:3 on $24k$, 98:2 on $16i$, and 54:46 on $6c$ for **6** follow the reduced amount of Zn.

Figure 3. View of the polyanionic framework of clathrates with type-I structure (yellow: pentagonal dodecahedra; purple: tetrakaidecahedra).



All guest atoms are located in the center of the polyhedra with usual anisotropic displacement parameters (see Figure 4). Both kinds of cavities are closer in size than for the type-II clathrates, yet, a strict ordering occurs again in the Cs-containing clathrate **4** with only Na atoms in the pentagon dodecahedra on site $2a$ and Cs atoms in the tetrakaidecahedra on site $6d$. In contrast, the polyhedra sizes are not so unambiguous for both Rb-containing clathrates. Hence, the $(\text{Si},\text{Ga})_{20}$ cavities in **5** are large enough for the Rb cations and a statistical mixed occupancies occurs with a ratio of $\text{Na}_2:\text{Rb}_2 = 83:17$, while only Rb cations are in the $(\text{Si},\text{Ga})_{24}$ cavities. In the Zn-containing clathrate **6**, the tetrakaidecahedra are already too small to encapsulate only Rb cations, resulting in a mixed occupancy of $\text{Rb}_1:\text{Na}_1$ with the ratio 86:14, and the pentagon dodecahedra are filled completely with Na atoms.

Figure 4. Representation of the polyhedral cages in the type-I structures with anisotropic displacement parameters, drawn at the 95% probability level. (a) $\text{Cs}_6\text{Na}_2\text{Ga}_{8.25}\text{Si}_{37.75(3)}$; (b) $\text{Rb}_{6.34}\text{Na}_{1.66(2)}\text{Ga}_{8.02}\text{Si}_{37.98(3)}$; and (c) $\text{Rb}_{5.20}\text{Na}_{2.80(4)}\text{Zn}_{3.85}\text{Si}_{42.15(2)}$.



The dependence of content and size of the framework building atoms is once more visible in the decreasing intervals for the distances (see Table 8) with $d_{\text{Si/Ga-Si/Ga}} = 2.395(1)\text{--}2.481(1)$ Å, $d_{\text{Na-Si/Ga}} = 3.334(1)\text{--}3.407(1)$ Å, $d_{\text{Cs-Si/Ga}} = 3.555(1)\text{--}4.035(1)$ Å for **4**, $d_{\text{Si/Ga-Si/Ga}} = 2.384(2)\text{--}2.465(1)$ Å, $d_{\text{Na2/Rb2-Si/Ga}} = 3.331(1)\text{--}3.410(1)$ Å, $d_{\text{Rb1-Si/Ga}} = 3.538(1)\text{--}4.031(1)$ Å for **5**, and $d_{\text{Si/Ga-Si/Ga}} = 2.378(1)\text{--}2.444(1)$ Å, $d_{\text{Na2-Si/Ga}} = 3.293(1)\text{--}3.381(1)$ Å, $d_{\text{Rb1/Na1-Si/Ga}} = 3.503(1)\text{--}4.002(1)$ Å for **6** as well as for the ternary clathrates $\text{Rb}_8\text{Ga}_8\text{Si}_{38}$ ($d_{\text{Si/Ga-Si/Ga}} = 2.365(1)\text{--}2.494(1)$ Å, $d_{\text{Rb2-Si/Ga}} = 3.351(1)\text{--}3.437(1)$ Å, $d_{\text{Rb1-Si/Ga}} = 3.540(1)\text{--}4.030(1)$ Å) [11] and $\text{K}_8\text{Ga}_{7.9}\text{Si}_{38.1}$ ($d_{\text{Si/Ga-Si/Ga}} = 2.366(1)\text{--}2.463(1)$ Å, $d_{\text{K2-Si/Ga}} = 3.332(1)\text{--}3.418(1)$ Å, $d_{\text{K1-Si/Ga}} = 3.523(1)\text{--}4.025(1)$ Å) [10] and in good agreement with the bond lengths of the corresponding type-II clathrates (*vide supra*).

Table 8. Selected interatomic distances for $\text{Cs}_6\text{Na}_2\text{Ga}_{8.25}\text{Si}_{37.75(3)}$ (**4**); $\text{Rb}_{6.34}\text{Na}_{1.66(2)}\text{Ga}_{8.02}\text{Si}_{37.98(3)}$ (**5**); and $\text{Rb}_{5.20}\text{Na}_{2.80(4)}\text{Zn}_{3.85}\text{Si}_{42.15(2)}$ (**6**). *Tt* denotes the mixed occupied Si/Ga and Si/Zn, respectively.

| Compound 4 | <i>d</i> /Å | Compound 5 | <i>d</i> /Å | Compound 6 | <i>d</i> /Å |
|----------------------|-------------|---------------------------|-------------|--------------------------|-------------|
| <i>Tt1-Tt2</i> (2×) | 2.3949(6) | <i>Tt1-Tt2</i> (2×) | 2.3991(5) | <i>Tt1-Tt2</i> (2×) | 2.3784(4) |
| <i>Tt1-Tt1</i> | 2.478(2) | <i>Tt1-Tt1</i> | 2.465(1) | <i>Tt1-Tt1</i> | 2.432(1) |
| <i>Tt1-Tt3</i> | 2.4807(8) | <i>Tt1-Tt3</i> | 2.4653(7) | <i>Tt1-Tt3</i> | 2.4440(6) |
| <i>Tt2-Tt2</i> | 2.3949(6) | <i>Tt2-Tt2</i> | 2.384(2) | <i>Tt2-Tt2</i> | 2.3784(4) |
| <i>Tt2-Tt1</i> (3×) | 2.399(2) | <i>Tt2-Tt1</i> (3×) | 2.3991(5) | <i>Tt2-Tt1</i> (3×) | 2.381(2) |
| <i>Tt3-Tt1</i> (4×) | 2.4807(8) | <i>Tt3-Tt1</i> (4×) | 2.4654(7) | <i>Tt3-Tt1</i> (4×) | 2.4440(6) |
| Cs- <i>Tt1</i> (8×) | 3.5552(5) | Rb1- <i>Tt1</i> (8×) | 3.5377(5) | Rb1/Na1- <i>Tt1</i> (8×) | 3.5025(4) |
| Cs- <i>Tt2</i> (8×) | 3.8916(4) | Rb1- <i>Tt2</i> (8×) | 3.8811(3) | Rb1/Na1- <i>Tt2</i> (8×) | 3.8465(3) |
| Cs- <i>Tt3</i> (4×) | 3.702(1) | Rb1- <i>Tt3</i> (4×) | 3.6934(1) | Rb1/Na1- <i>Tt3</i> (4×) | 3.6608(1) |
| Cs- <i>Tt1</i> (4×) | 4.0352(8) | Rb1- <i>Tt1</i> (4×) | 4.031(1) | Rb1/Na1- <i>Tt1</i> (4×) | 4.002(1) |
| Na- <i>Tt2</i> (8×) | 3.334(1) | Na2/Rb2- <i>Tt2</i> (8×) | 3.331(1) | Na- <i>Tt2</i> (8×) | 3.2932(7) |
| Na- <i>Tt1</i> (12×) | 3.4066(8) | Na2/Rb2- <i>Tt1</i> (12×) | 3.4103(7) | Na- <i>Tt1</i> (12×) | 3.3813(6) |

The refined formulae for the type-I clathrates are satisfying the Zintl-Klemm ideas for valence electrons counting and charge balance with $[(\text{Na,Cs or Rb})^+]_8[4b\text{-Ga}^1]_8[4b\text{-Si}^0]_{38}$ for $\text{Cs}_6\text{Na}_2\text{Ga}_{8.25}\text{Si}_{37.75(3)}$

and $\text{Rb}_{6.34}\text{Na}_{1.66(2)}\text{Ga}_{8.02}\text{Si}_{37.98(3)}$, and $[(\text{Na},\text{Rb})^+]_8[4b\text{-Zn}^{2-}]_4[4b\text{-Si}^0]_{42}$ for $\text{Rb}_{5.20}\text{Na}_{2.80(4)}\text{Zn}_{3.85}\text{Si}_{42.15(2)}$, hence, semiconducting behavior can be expected for all three compounds. Given this and the robust open framework with many possibilities for substitutions, such compounds could be candidate-materials for thermoelectric applications. However, these speculations could not be confirmed as part of this study, as the synthesis requirements for phase-pure sample have not been yet worked out.

3. Experimental Section

3.1. Synthesis

Due to the high reactivity of the alkali metals in air, all manipulations involving elemental Na, Rb, and Cs were carried out in a glove box with $\text{O}_2/\text{H}_2\text{O}$ level below 1 ppm or under vacuum. All chemicals were purchased from Alfa or Sigma-Aldrich with purity higher than 99.9%.wt. In order to carry out the reactions in a safe and reliable manner, the elements were loaded in a ratio of $\text{Na}:A:M:\text{Si} = 2:1:3:14$ ($A = \text{Rb}, \text{Cs}$; $M = \text{Ga}, \text{Zn}$) in Nb tubes (4.5 cm long, diameter 1 cm). After arc sealing and enclosing of the tubes in evacuated, fused silica jackets, the samples were heated slowly in programmable muffle furnaces to 950 °C with a rate of 10 °C/h, annealed for 15 h, and then cooled down (rate -150 °C/h) to 650 °C, dwelled for 4 d, and cooled down (rate -5 °C/h) to room temperature. The obtained type-I and type-II clathrates are stable in air and moisture for a couple of months. Leftover Si can be washed out with 1 M NaOH-solution.

In all systems, variations of the loading ratio for the idealized formulae (type-I and type-II) as well as of the temperature profiles (reaction temperatures varied between 600 and 950 °C) resulted only in small changes of the ratios of the clathrate types and leftover Si. The same three-phase product occurs (i) if the reactions (stoichiometric loadings in Nb tubes) are performed with induction heating at temperatures between 800 and 900 °C for 10 min or (ii) if the flux method is used. For the latter one, a ten-fold excess of Ga or Zn, respectively, were used as flux. The samples were loaded in Nb tubes (8 cm long, diameter 1 cm, and an Nb sheet with drilled hollows is inserted as filter part), enclosed in evacuated silica tubes, heated to 800 °C (rate 100 °C/h), annealed for 2 h and then cooled down with a rate of -2 °C/h. Subsequently, the flux was removed at 300 °C.

Analogous reactions in the system Cs-Na-Zn-Si may have produced the type-II clathrate $\text{Cs}_8\text{Na}_{16}\text{Zn}_x\text{Si}_{136-x}$, but this supposition from powder X-ray diffraction data is not yet confirmed from structure refinements by single-crystal work. The major products of the reaction appear to be NaZn_{13} and unreacted Si. There is no experimental evidence suggesting that type-I compound can be obtained in this system. More work is required and future results will be published elsewhere.

Independent from the type of synthesis method employed, the obtained single-crystals were small and normally intergrown together. The crystals were cuboidal in shape with dark-to-black appearance. Both type-I and type-II had the same morphology and could not be distinguished under a microscope. The typical size of the single-crystals was below $0.1 \times 0.1 \times 0.1$ mm, and, therefore, property measurements on individual crystallites also could not be carried out.

3.2. Single Crystal X-ray Diffraction

Single-crystal X-ray diffraction data were collected on a Bruker Smart Apex diffractometer at 200 K using graphite-monochromated Mo-K α radiation ($\alpha = 0.71073 \text{ \AA}$). Suitable single crystals of each compound were selected and cut to smaller dimensions (less than 0.1 mm) under mineral oil. The *SMART* [28] and *SAINTPplus* [29] programs were used for the data collection, integration and the global unit cell refinement from all data. Semi-empirical absorption correction was applied with *SADABS* [30]. The structures were refined to convergence by full matrix least-square methods on F^2 , as implemented in *SHELXTL* [31]. All sites were refined with anisotropic displacement parameters. The atomic parameters were standardized with *StructureTidy* as implemented in *Platon* [32].

The contrast between the X-ray atomic scattering factors between Zn, Ga and Si, respectively, is significant enough to allow precise refinements of the site occupation factors. In all cases, the occupancies of the framework sites were first freely refined (individually, while the remaining ones were kept fixed). For the type-II structures, the occupancies of all three Si/ M ($M = \text{Ga, Zn}$) showed mixed occupation, except for $\text{Rb}_8\text{Na}_{16}\text{Zn}_{8.4}\text{Si}_{127.6(1)}$, where Zn was found only on framework sites 96g and 32e. Notably, the largest amount of Ga or Zn was found at the site with the lowest symmetry index (96g), while the completely opposite observations can be made for the type-I structures—in these cases, all three framework sites are co-occupied, with a noted preference for the site with the highest symmetry (6c). In all three type-I clathrates, small amounts of Ga and Zn, respectively, co-occupy framework sites 16i and 24k as well. This situation is similar to $\text{Ba}_8\text{Zn}_7\text{Si}_{39}$ [33], in which sites 6c (77% Zn, 23% Si) and 24k (9% Zn, 91% Si) are mixed occupied. In the $\text{Ba}_8\text{Zn}_x\text{Ge}_{46-x-y}$ compounds with $2.1 \leq x \leq 7.7$ [34], the Zn atoms are suggested not to occupy the other site(s) until site 6c is completely filled by Zn. Such assertion pertaining to low framework substitution levels is interesting and warrants further exploration, however, the refinements of Zn/Ge may not be as accurate as Zn/Si due to the better contrast in their X-ray scattering factors.

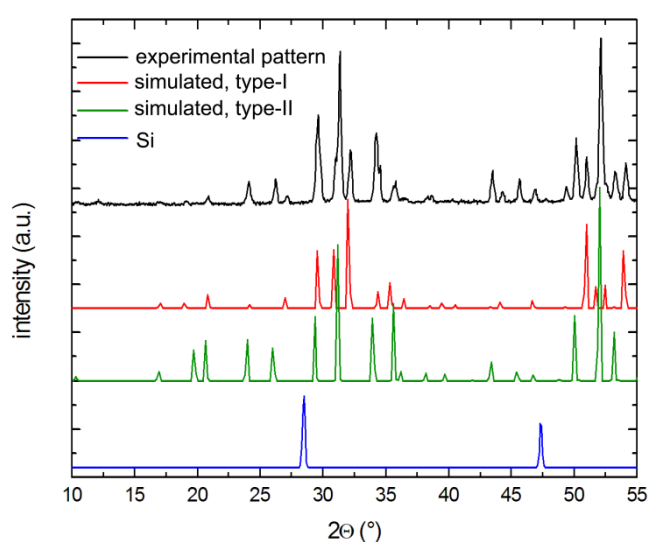
The individual ratios of the statistical mixed order are compiled in Tables 2 and 6. Hints for vacancies in the framework (e.g., low occupation factors, elongated displacement parameters of atoms neighboring possible vacant sites, etc.) are not observed for any compound. The guest atoms are always located in the center of the respective cavities (16c and 8b for type-II, and 6d and 2a for type-I, respectively) and the values for the anisotropic displacement parameters do not indicate any kind of off-centering.

Selected details of the data collections and structure refinement parameters are listed in Tables 1 and 5. The atomic coordinates and equivalent isotropic displacement parameters are compiled in Tables 2 and 6. The anisotropic displacement parameters can be found in Tables 3 and 7 and selected interatomic distances are summarized in Tables 4 and 8. Additional details of the crystal structure analyses may be requested from the Fachinformationszentrum Karlsruhe, D-76344 Eggenstein-Leopoldshafen, Germany (Fax: +49-7247-808-666, E-Mail: crysdata@fiz-karlsruhe.de) on quoting the depository numbers CSD-427236 for $\text{Cs}_8\text{Na}_{16}\text{Ga}_{22.7}\text{Si}_{113.3(1)}$, CSD-427237 for $\text{Rb}_{8.4}\text{Na}_{15.6(1)}\text{Ga}_{19.6}\text{Si}_{116.4(1)}$, CSD-427238 for $\text{Rb}_8\text{Na}_{16}\text{Zn}_{8.4}\text{Si}_{127.6(1)}$, CSD-427239 for $\text{Cs}_6\text{Na}_2\text{Ga}_{8.25}\text{Si}_{37.75(3)}$, CSD-427240 for $\text{Rb}_{6.34}\text{Na}_{1.66(2)}\text{Ga}_{8.02}\text{Si}_{37.98(3)}$, and CSD-427241 for $\text{Rb}_{5.20}\text{Na}_{2.80(4)}\text{Zn}_{3.85}\text{Si}_{42.15(2)}$, respectively.

3.3. Powder X-ray Diffraction

X-ray powder diffraction patterns of selected crystals were carried out at room temperature on a Rigaku MiniFlex powder diffractometer using Cu-K α radiation. Typical runs included θ – θ scans ($2\theta_{\max} = 65^\circ$) with the scan steps of 0.05° and 2 s/step counting time. The data were analyzed with the JADE 6.5 software package [35]. The intensities and the positions of the experimentally observed peaks and those calculated based on the corresponding single-crystal structures matched very well with one another (see Figure 5).

Figure 5. Representative powder x-ray pattern of a Cs-containing sample after soaking in 1 M NaOH solution. Both clathrates types are detected, while Si is dissolved completely.



3.4. EDX Analysis

Multiple crystals for each composition were also determined by means of energy dispersive X-ray spectroscopy (EDX) on a JEOL 7400F electron microscope equipped with an INCA-OXFORD energy-dispersive spectrometer. All four elements could be detected in ratios consistent with the refined compositions, however precise quantitative analyses were hampered due to the strong overlay of the lines for Si/Rb and Na/Ga or Na/Zn, respectively.

4. Conclusions

In all three studied systems: Cs–Na–Ga–Si, Rb–Na–Ga–Si, and Rb–Na–Zn–Si, the synthesis of type-I and type-II clathrates is proved possible. However, the respective clathrate phases are always co-crystallizing in the same sample batches, irrespective of the tried different synthesis routes (stoichiometric reactions with long-time annealing in muffle furnaces or with short-time heating in induction furnaces as well as flux reactions). As mechanical separation was not achievable either, measurements of the transport properties could not be performed. Another problem that calls for further investigation is the mixed occupancies of the cavities in the Rb-containing clathrates. A control over the composition seems only be possible for the Cs clathrates due to the strict filling of the cavities

and, therefore, resulting in nearly line compounds. Thus, this system can prove the most promising if the synthetic problems leading to impurity phases can be resolved in further investigations.

Acknowledgments

The authors gratefully acknowledge financial support from the US Department of Energy through grants DE-SC0001360 and DE-SC0008885.

Conflicts of Interest

The authors declare no conflict of interest.

References and Notes

1. Jeffrey, G.A. Hydrate Inclusion Compounds. In *Inclusion Compounds*; Atwood, I.J.L., Davies, J.E.D., MacNicol, D.D., Eds.; Academic Press: London, UK, 1984; pp. 135–190.
2. Slack, G.A. New Materials and Performance Limits for Thermoelectric Cooling. In *CRC Handbook of Thermoelectrics*; Rowe, D.M., Ed.; CRC Press: Boca Raton, FL, USA, 1995; pp. 407–440.
3. Nolas, G.S.; Cohn, J.L.; Slack, G.A.; Schjuman, S.B. Semiconducting Ge clathrates: Promising candidates for thermoelectric applications. *Appl. Phys. Lett.* **1998**, *73*, 178–180.
4. Sales, B.C.; Chakoumakos, B.C.; Mandrus, D.; Sharp, J.W. Atomic displacement parameters and the lattice thermal conductivity of clathrate-like thermoelectric compounds. *J. Solid State Chem.* **1999**, *146*, 528–532.
5. Christensen, M.; Johnson, S.; Iversen, B.B. Thermoelectric clathrates of type-I. *Dalton Trans.* **2010**, *39*, 978–992.
6. Bobev, S.; Sevov, S.C. Clathrates of group 14 with alkali metals: An exploration. *J. Solid State Chem.* **2000**, *153*, 92–105.
7. Beekman, M.; Nolas, G.S. Inorganic clathrate-II materials of group 14: Synthesis routes and physical properties. *J. Mater Chem.* **2008**, *18*, 842–851.
8. Shevelkov, A.V.; Kovnir, K. Zintl Clathrates. In *Structure and Bonding*; Springer: Berlin, Germany, 2011; Volume 990, pp. 97–142.
9. Prokofiev, A.; Sidorenko, A.; Hradil, K.; Ikeda, M.; Svagera, R.; Waas, M.; Winkler, H.; Neumaier, K.; Paschen, S. Thermopower enhancement by encapsulating cerium in clathrate cages. *Nature Mater.* **2013**, *12*, 1096–1101.
10. Kröner, R.; Peters, K.; von Schnering, H.G.; Nesper, R. Crystal structure of the clathrates $K_8Ga_8Si_{38}$ and $K_8Ga_8Sn_{38}$. *Z. Kristallogr.* **1998**, *231*, 667–668.
11. Von Schnering, H.G.; Kröner, R.; Menke, H.; Peters, K.; Nesper, R. Crystal structure of the clathrates $Rb_8Ga_8Sn_{38}$, $Rb_8Ga_8Ge_{38}$ and $Rb_8Ga_8Si_{38}$. *Z. Kristallogr.* **1998**, *213*, 677–678.
12. Paschen, S.; Budnyk, S.; Köhler, U.; Prots, Y.; Hiebl, K.; Steglich, F.; Grin, Y. New type-I clathrates with ordered Eu distribution. *Physica B* **2006**, *383*, 89–92.
13. Von Schnering, H.G.; Menke, H.; Kröner, R.; Peters, E.M.; Peters, K.; Nesper, R. Crystal structure of the clathrates $Rb_8In_8Ge_{38}$ and $K_8In_8Ge_{38}$. *Z. Kristallogr.* **1998**, *213*, 673–374.

14. Schäfer, M.C.; Bobev, S. On the possibility for Rb- and Eu-cation ordering in type-I clathrates. Synthesis and homogeneity range of the novel compounds $\text{Rb}_{8-x}\text{Eu}_x(\text{In,Ge})_{46}$ ($0.6 \leq x \leq 1.8$). *Acta Crystallogr.* **2013**, *C69*, 1457–1461.
15. Bobev, S.; Sevov, S.C. Synthesis and characterization of stable stoichiometric clathrates of silicon and germanium: $\text{Cs}_8\text{Na}_{16}\text{Si}_{136}$ and $\text{Cs}_8\text{Na}_{16}\text{Ge}_{136}$. *J. Am. Chem. Soc.* **1999**, *121*, 3795–3796.
16. Nolas, G.S.; Vanderveer, D.G.; Wilkinson, A.P.; Cohn, J.L. Temperature dependent structural and transport properties of the clathrates $\text{A}_8\text{Na}_{16}\text{E}_{136}$ (A = Cs or Rb and E = Ge or Si). *J. Appl. Phys.* **2002**, *91*, 8970–8973.
17. Bobev, S.; Meyers, J., Jr.; Fritsch, V.; Yamasaki, Y. Synthesis and structural characterization of novel clathrate-II compounds of silicon. In Proceedings of the 25th International Conference on Thermoelectrics, Vienna, Austria, 6–10 August 2006; IEEE: New York, NY, USA, 2006; Volume 25, pp. 48–52.
18. Beekman, M.; Wong-Ng, W.; Kaduk, J.A.; Shapiro, A.; Nolas, G.S. Synthesis and single-crystal X-ray diffraction studies of new framework substituted type II clathrates, $\text{Cs}_8\text{Na}_{16}\text{Ag}_x\text{Ge}_{136-x}$ ($x < 7$). *J. Solid State Chem.* **2007**, *180*, 1076–1082.
19. Beekman, M.; Kaduk, J.A.; Gryko, J.; Wong-Ng, W.; Shapiro, A.; Nolas, G.S. Synthesis and characterization of framework-substituted $\text{Cs}_8\text{Na}_{16}\text{Cu}_5\text{Ge}_{131}$. *J. Alloys Compd.* **2009**, *470*, 365–368.
20. Schäfer, M.C.; Bobev, S. Novel tin clathrates with the type-II structure. *J. Am. Chem. Soc.* **2013**, *135*, 1696–1699.
21. Beekman, M.; Baitinger, M.; Borrmann, H.; Schnelle, W.; Meier, K.; Nolas, G.S.; Grin, Y. Preparation and crystal growth of $\text{Na}_{24}\text{Si}_{136}$. *J. Am. Chem. Soc.* **2009**, *131*, 9642–9643.
22. Beekman, M.; Nenghasi, E.N.; Biswas, K.; Myles, C.W.; Baitinger, M.; Grin, Y.; Nolas, G.S. Framework contraction in Na-stuffed $\text{Si}(c\text{F}136)$. *Inorg. Chem.* **2010**, *49*, 5338–5340.
23. Stefanoski, S.; Beekman, M.; Wong-Ng, W.; Zavalij, P.; Nolas, G.S. Simple approach for selective crystal growth of intermetallic clathrates. *Chem. Mater.* **2011**, *23*, 1491–1495.
24. Some progress has made here in the selective synthesis of phase-pure type-I $\text{Na}_8\text{Si}_{46}$ and type-II $\text{Na}_{24-x}\text{Si}_{136}$ ($0 \leq x \leq 24$) by controlled thermal decomposition of Na_4Si_4 (as a precursor) using spark plasma sintering ref. [21] or vapor pressure refs. [22,23], allowing even for control over the Na content, but the application of this method has so far been limited to the Na–Si binary phase diagram.
25. Pauling, L. *The Nature of the Chemical Bonding*, 3rd ed.; Cornell University Press: Ithaca, NY, USA, 1960; p. 403.
26. Miller, G.J. Structure and Bonding at the Zintl Border. In *Chemistry, Structure, and Bonding of Zintl Phases and Ions*; Kauzlarich, S., Ed.; VCH: New York, NY, USA, 1996; pp. 1–57.
27. Guloy, A.M. Polar Intermetallics and Zintl Phases along the Zintl Border. In *Inorganic Chemistry in Focus III*; Meyer, G., Naumann, D., Wesemann, L., Eds.; Wiley-VCH: Weinheim, Germany, 2006; pp. 157–172.
28. *SMART NT, Version 5.63*; Bruker Analytical X-ray Systems Inc.: Madison, WI, USA, 2003.
29. *SAINT NT, Version 6.45*; Bruker Analytical X-ray Systems Inc.: Madison, WI, USA, 2003.
30. *SADABS NT, Version 2.10*; Bruker Analytical X-ray Systems Inc.: Madison, WI, USA, 2001.
31. *SHELXTL, Version 6.12*; Bruker Analytical X-ray Systems Inc.: Madison, WI, USA, 2001.

32. *PLATON, Version 1.15*; Spek, A.L., Ed.; Utrecht University: Utrecht, The Netherlands, 2008.
33. Nasir, N.; Grytsiv, A.; Melnychenko-Koblyuk, N.; Rogl, P.; Bauer, E.; Lackner, R.; Royanian, E.; Giester, G.; Saccone, A. Clathrates $\text{Ba}_8\{\text{Zn,Cd}\}_x\text{Si}_{46-x}$, $x \sim 7$: Synthesis, crystal structure and thermoelectric properties. *J. Phys.* **2009**, *21*, 385404.
34. Melnychenko-Koblyuk, N.; Grytsiv, A.; Fornasari, L.; Kaldarar, H.; Michor, H.; Roehrbacher, F.; Koza, M.; Royanian, E.; Bauer, E.; Rogl, P.; *et al.* Ternary clathrates Ba–Zn–Ge: Phase equilibria, crystal chemistry and physical properties. *J. Phys.* **2007**, *19*, 216223.
35. *JADE, Version 6.5*; Materials Data, Inc.: Livermore, CA, USA, 2003.

© 2014 by the authors; licensee MDPI, Basel, Switzerland. This article is an open access article distributed under the terms and conditions of the Creative Commons Attribution license (<http://creativecommons.org/licenses/by/3.0/>).